Reliability Engineering and System Safety 115 (2013) 43–54

Contents lists available at SciVerse ScienceDirect

Reliability Engineering and System Safety

journal homepage: www.elsevier.com/locate/ress

Global sensitivity analysis of the impact of impurities on CO_2 pipeline failure

S. Brown [a], J. Beck [b,*], H. Mahgerefteh [a], E.S. Fraga [b,c]

[a] Department of Chemical Engineering, University College London, London WC1E 7JE, UK
[b] Centre for Process Systems Engineering, Department of Chemical Engineering, University College London, London WC1E 7JE, UK
[c] School of Energy and Resources, UCL Australia, University College London, Adelaide, SA 5000, Australia

ARTICLE INFO

Article history:
Received 7 September 2012
Received in revised form
23 January 2013
Accepted 7 February 2013
Available online 27 February 2013

Keywords:
Global sensitivity analysis
Generalised polynomial chaos
Sparse grid
Uncertainty quantification
CO_2 pipeline failure
Failure consequence analysis

ABSTRACT

This paper describes the testing, comparison and application of global sensitivity techniques for the study of the impact of the stream impurities on CO_2 pipeline failure. Global sensitivity analysis through non-intrusive generalised polynomial chaos expansion with sparse grids is compared to more common techniques and is found to achieve superior convergence rate to crude Monte Carlo, quasi-Monte Carlo and EFAST for functions with up to a moderate level of "roughness". This methodology is then applied to the hypothetical full bore rupture of a 1 km CO_2 pipeline at 150 bara and 283.15 K. The sensitivity of the ensuing outflow to the composition of a quaternary mixture of CO_2 with N_2, CH_4 and O_2 as representative stream impurities. The results indicate that the outflow rate is highly sensitive to the composition during the early stages of depressurisation, where the effect of the impurities on phase equilibria has a significant impact on the outflow.

1. Introduction

As part of the carbon capture and sequestration (CCS) chain, pressurised pipelines are considered to be the most practical and efficient means for transportation of the large amounts of CO_2 captured from fossil fuel power plants for subsequent sequestration [22]. It is inevitable that such pipelines will cover distances of several hundreds of kilometres, possibly at line pressures above 100 bar. Given that CO_2 gas is an asphyxiant at concentrations higher than 7% [25], the safety of CO_2 pipelines is of paramount importance and indeed pivotal to the public acceptability of CCS as a viable means for tackling the impact of global warming [22].

The outflow and its variation with time following pipeline failure dictates the resulting atmospheric dispersion of the escaping inventory, an example of which can be observed in Fig. 1. These data govern all the consequences associated with the pipeline failure, including minimum safe distances to populated areas and emergency response planning.

Naturally a great deal of uncertainty is present due to the many possible circumstances in which a failure occurs including failure type, i.e. puncture or full bore rupture, initial failure pressure and temperature and variations in the captured stream composition due to fluid stream sources based on differing capture methods (i.e. pre-combustion, post-combustion or oxyfuel) [12] and post-capture processing. The use of predictive models to examine the sensitivity of the consequences of pipeline failure to these variations is standard within a quantitative risk assessment [23]. Such an analysis is often conducted using a one-factor-at-a-time (OAT) methodology [23,47], but as discussed by Saltelli and Annoni [35] this technique assumes an underlying linear behaviour, which is unlikely to be the case in such complex systems. To avoid such an assumption about the underlying model, a global sensitivity analysis (GSA) is required.

GSA is concerned with quantifying how the variation in the model's output depends on different sources of variation over the entire parameter space, here treated as random input data, by providing quantitative importance measures that relate the variance of the output with each input variable. This form of analysis of model sensitivity has been applied to parts of the CCS chain, to the geological storage of CO_2 by Kovscek and Wang [24] where the effect of porosity and permeability on reservoir performance was assessed, and widely applied in environmental engineering. For example, Cea et al. [10] studied the effects of aleatoric and epistemic uncertainty on a water quality model for evaluating biological pollutant concentration.

Given the complexity of the fluid and thermodynamic behaviour of the flow following a pipeline failure, substantial resources are required for its computation [28], and as a result, the application of GSA has been considered impractical. However, the success of recent work [6,28] to decrease the computational expense of each simulation enables one to calculate the total sensitivities.

In this work GSA is applied using a sensitivity measure proposed by Sobol' [41] to gain a better understanding of the effect of impurities on the outflow following pipeline failure.

* Corresponding author. Tel.: +44 20 7679 3809.
E-mail address: joakim.back.09@ucl.ac.uk (J. Beck).

0951-8320/$ - see front matter © 2013 Elsevier Ltd. All rights reserved.
http://dx.doi.org/10.1016/j.ress.2013.02.006

Fig. 1. CO_2 outflow and dispersion during pipeline decompression courtesy of Dalian University.

The Sobol' method is related to analysis of variance (ANOVA) and decomposes the model variation into a number of effects that represent the influence of each input, represented by a probability distribution, and their interactions. Many methods have been proposed to compute the integrals required to calculate these effects, of these the most widely applied are Monte Carlo sampling and the Extended Fourier Amplitude Sensitivity Test (EFAST) [30]. These approaches usually require large sample sizes to provide accurate estimations of the sensitivities, making them impractical when the underlying model is computationally expensive.

Sudret [44] proposed a procedure for the computation of the Sobol' sensitivity measures through the approximation of the model's output by a polynomial expansion, known as generalised polynomial chaos (gPC) [19]. The gPC expansion is a linear combination of suitable global polynomial approximations in probability space, for which the statistical moments, expected value and variance, are known *exactly* from the coefficients of the expansion (see also [13,16]). The family of orthonormal mono-dimensional polynomials is selected in accordance with the general Askey scheme [50] with respect to the probability measure of each random input variable. The gPC expansion may be constructed intrusively by a Galerkin projection reformulation of the underlying problem or through non-intrusive approaches such as projection and regression (see [5,45]).

In recent years stochastic collocation [4,49] has been applied to build *sparse* gPC expansions on tensor grids for high dimensional random input data (see e.g. [9]), to mitigate the so-called "Curse of Dimensionality". This method constructs an approximative function that is a sum of Lagrangian interpolants on a set of points, which is known as a *sparse grid* (see [8]) (originally introduced by Smolyak [39] for multi-dimensional integration). The approximative function can be converted into the form of a gPC expansion. Formaggia et al. [18] applied GSA with gPC expansion derived from the stochastic collocation method to a basin-scale geochemical compaction model and advocated its applicability to models subject to high dimensional random input data. This sparse gPC expansion potentially requires far fewer function evaluations than the other methods identified above, meaning that the use of GSA for complex numerical models, such as that required for modelling the discharge following pipeline failure, may be tractable.

The paper is organised as follows. Section 2 presents a review of a particular decomposition of a multi-variate function (Section 2.2). It is then shown how this expansion is used to define the Sobol' sensitivity indices (Section 2.3) and a number of common methods (i.e. Monte Carlo, EFAST and gPC) for calculating the Sobol' indices are presented. These methodologies are then tested against two benchmark test functions, and a family of test functions constructed to investigate the robustness of gPC (Section 2.4). The test functions constructed exhibit near discontinuous behaviour, and further difficulty is induced with additive artificial white noise. In Section 3 the most efficient of these techniques, in terms of convergence per number of function evaluations, is applied to a pipeline failure scenario. An extensively validated pipeline decompression model is presented in Section 3.1, while the uncertainty in the likely composition of a CO_2 stream is discussed in Section 3.2. Firstly, Monte Carlo simulation is used to estimate the outcome probability distribution and perform a crude sensitivity analysis with scatter plotting. The final analysis serves as a framework for future work on consequence analysis for pipeline failure under uncertainty. Finally conclusions resulting from this work are drawn in Section 4.

2. Global sensitivity analysis

2.1. Probabilistic formulation

Let $\mathbf{y}(\omega)=(y_1(\omega),y_2(\omega),\ldots,y_n(\omega),\ldots,y_N(\omega)):\Omega\rightarrow\mathbb{R}^N$ represent N independent and identically distributed (i.i.d.) random variables, $\Gamma_n\subseteq\mathbb{R}$ the image set of the random variable y_n, and $\Gamma=\prod_{n=1}^{N}\Gamma_n$. Hence the joint probability distribution function $\rho:\Gamma\rightarrow\mathbb{R}$ of $\mathbf{y}$ can be factorised as $\rho(\mathbf{y})=\Pi_{n=1}^{N}\rho(y_n)$, where $\rho(y_n)$ is the marginal probability distribution function of y_n. Let $(\Gamma,\mathrm{B}(\Gamma),\rho(\mathbf{y})\,\mathrm{d}\mathbf{y})$, where $\mathrm{B}(\Gamma)$ is the Borel σ-algebra on Γ, and $\rho(\mathbf{y})\,\mathrm{d}\mathbf{y}$ is the probability distribution measure of $\mathbf{y}$ on Γ. $L^2_\rho(\Gamma)$ denotes the Hilbert space consisting of square integrable functions on Γ with respect to the measure $\rho(\mathbf{y})\,\mathrm{d}\mathbf{y}$.

2.2. Functional ANOVA representation

A function $u\in L^2_\rho(\Gamma)$ can be expanded as a functional ANOVA decomposition

$$u(\mathbf{y})=u_{\mathbf{0}}+\sum_{\mathbf{j}\subseteq\mathcal{J}}u_{\mathbf{j}}(\mathbf{y}_{\mathbf{j}}), \tag{1}$$

for which $\mathbf{y}_{\mathbf{j}}=(y_{j_1},y_{j_2},\ldots,y_{j_{|\mathbf{j}|}})$ is a vector including the components of $\mathbf{y}$ indexed by $\mathbf{j}$, where $\mathbf{j}$ represents a non-empty subset of the coordinate indices $\mathcal{J}=\{1,\ldots,N\}$ with cardinality denoted by $|\mathbf{j}|$. For example, for $\mathbf{j}=\{2,3\}$ and $\{1,3,4\}$, $|\mathbf{j}|=2$ and 3, respectively. Let $\Gamma^{\mathbf{j}}$ denote the $|\mathbf{j}|$-dimensional hyper-rectangle defined as the projection of the N-dimensional Γ onto the hyper-rectangle indexed by $\mathbf{j}$. The ANOVA representation allows one to distinguish between first order effects, low-order interdependence, and high-order interaction. The summands $u_{\mathbf{j}}(\mathbf{y}_{\mathbf{j}})$ can be calculated recursively as follows:

$$u_{\mathbf{0}}=\int_{\Gamma^N}u(\mathbf{y})\rho(\mathbf{y})\,\mathrm{d}\mathbf{y} \tag{2}$$

and

$$u_{\mathbf{j}}(\mathbf{y}_{\mathbf{j}})=\int_{\Gamma^{N-|\mathbf{j}|}}u(\mathbf{y})\rho(\mathbf{y}_{\sim\mathbf{j}})\,\mathrm{d}\mathbf{y}_{\sim\mathbf{j}}-\sum_{\mathbf{k}\subset\mathbf{j}}u_{\mathbf{k}}(\mathbf{y}_{\mathbf{k}})-u_{\mathbf{0}}. \tag{3}$$

The measure $\rho(\mathbf{y}_{\sim\mathbf{j}})\,\mathrm{d}\mathbf{y}_{\sim\mathbf{j}}$ represents the integration over $\Gamma^{\sim\mathbf{j}}$. The ANOVA expansion is an exact projection of u with respect to the $L^2_\rho(\Gamma)$-inner product onto the mutually orthogonal $u_{\mathbf{j}}$, $\mathbf{j}\subseteq\mathcal{J}$, that is,

$$\int_\Gamma u_{\mathbf{j}}(\mathbf{y}_{\mathbf{j}})u_{\mathbf{k}}(\mathbf{y}_{\mathbf{k}})\rho(\mathbf{y})\,\mathrm{d}\mathbf{y}=\delta_{\mathbf{jk}}, \tag{4}$$

in which $\delta_{\mathbf{jk}} \neq 0$ if $\mathbf{j} = \mathbf{k}$, else $\delta_{\mathbf{jk}} = 0$. Hence it holds that for all $|\mathbf{j}| > 0$,

$$\int_{\Gamma} u_{\mathbf{j}}(\mathbf{y}_{\mathbf{j}})\rho(\mathbf{y})\,\mathrm{d}\mathbf{y} = 0. \tag{5}$$

2.3. Sobol' sensitivity indices

Sobol' [41] proposed a variance based GSA method that extends decomposition (1) to a variance based representation where the summands can be interpreted as relative importance measures of the subsets of the input variables. Following Eqs. (1), (4) and (5) the Sobol' indices are given by

$$S_{\mathbf{j}} = \frac{\mathbb{V}[u_{\mathbf{j}}(\mathbf{y}_{\mathbf{j}})]}{\mathbb{V}[u(\mathbf{y})]} = \frac{\int_{\Gamma} u_{\mathbf{j}}^2(\mathbf{y}_{\mathbf{j}})\rho(\mathbf{y})\,\mathrm{d}\mathbf{y}}{\int_{\Gamma} u^2(\mathbf{y})\rho(\mathbf{y})\,\mathrm{d}\mathbf{y} - u_{\mathbf{0}}^2}, \tag{6}$$

in which the variance of $u(\mathbf{y})$ under the probability measure $\rho(\mathbf{y})\,\mathrm{d}\mathbf{y}$ is

$$\mathbb{V}[u(\mathbf{y})] = \sum_{\mathbf{j} \subseteq \mathcal{J}} \mathbb{V}[u_{\mathbf{j}}(\mathbf{y}_{\mathbf{j}})] = \sum_{\mathbf{j} \subseteq \mathcal{J}} \int_{\Gamma} u_{\mathbf{j}}^2(\mathbf{y}_{\mathbf{j}})\rho(\mathbf{y})\,\mathrm{d}\mathbf{y}. \tag{7}$$

Accordingly, it holds that $\sum_{\mathbf{j} \subseteq \mathcal{J}} S_{\mathbf{j}} = 1$. It must be noted that Eq. (7) relies on the assumption of the mutual independence of $\{y_n\}$. The Sobol' indices quantify the relative importance of their corresponding effects which provide valuable insight on the mixed effects. The total effect induced by each input variable y_n has been defined by Homma and Saltelli [21] as

$$S_n^T = \sum_{\mathbf{j} \subseteq \mathcal{J} : n \in \mathbf{j}} S_{\mathbf{j}}. \tag{8}$$

The total effects S_n^T are in practice easy to compute through their complement in $\mathcal{J}$, that is, $S_{\mathbf{j}}$ for which $n \notin \mathbf{j}$. When underlying function evaluations are computationally expensive, a complete characterisation of all sensitivity indices is, in general, not feasible to compute.

2.3.1. Monte Carlo sampling

The Monte Carlo (MC) is a widely used sampling method to estimate multi-dimensional integrals. MC features a slow error convergence, the error is proportional to the work $m^{-(1/2)W}$, where m is the number of trials and W the work of a single trial evaluation. It does not exploit the possible regularity that the quantity of interest $u(\mathbf{y})$ might have with respect to the random input variables. Sobol' [41] showed that four MC computations are sufficient to compute the first order and total sensitivities:

$$\int_{\Gamma^N} u(\mathbf{y})\rho(\mathbf{y})\,\mathrm{d}\mathbf{y}, \quad \int_{\Gamma^N} u^2(\mathbf{y})\rho(\mathbf{y})\,\mathrm{d}\mathbf{y}, \tag{9}$$

$$\int_{\Gamma^{N-1}} u(\mathbf{y})u(\mathbf{y}_{\mathcal{J}\setminus\{n\}})\rho(\mathbf{y}_{\mathcal{J}\setminus\{n\}})\,\mathrm{d}\mathbf{y}_{\mathcal{J}\setminus\{n\}} \quad \text{and}$$

$$\int_{\Gamma^1} u(\mathbf{y})u(\mathbf{y}_{\{n\}})\rho(\mathbf{y}_{\{n\}})\,\mathrm{d}\mathbf{y}_{\{n\}}.$$

Quasi-Monte Carlo (QMC) sampling, using the Sobol' sequence LP_τ [40], for example, can also be used [42].

2.3.2. Fourier amplitude sensitivity test methods

The FAST (Fourier amplitude sensitivity test) method [30] reduces the following multi-dimensional integration:

$$\mathbb{E}[u(\mathbf{y})] = \int_{\Gamma^N} u(\mathbf{y})\rho(\mathbf{y})\,\mathrm{d}\mathbf{y} \tag{10}$$

to a one-dimensional integration along a curve by applying Weyl's theorem [46]. This is achieved by associating each variable y_n with a frequency ω_n of the system in the Fourier transform space, forming a set Ω. Each variable is then transformed by

$$y_n(s) = G_n(\sin(\omega_n s)), \quad n = 1, \ldots, N, \tag{11}$$

where G_n is an appropriate set of functions chosen such that Eq. (11) forms a space filling curve. Various transformations have been suggested (see e.g. [38]) for FAST. As an example,

$$y_n(s) = \frac{1}{2} + \frac{1}{\pi}\arcsin(\sin(\omega_n s)). \tag{12}$$

The Fourier coefficients associated with ω_n are then used as a measure of the sensitivity of the output function to input variable y_n. It was shown by Saltelli and Bolado [36] that this calculation is equivalent to that proposed by Sobol' for the first order sensitivities. Saltelli et al. [38] proposed an extension of FAST, called EFAST, that uses the first order effect estimates by FAST to compute total sensitivities, this is done by computing total sensitivities through the complement of the first order effects. To calculate the complement a random phase shift, $\psi_n \sim \mathcal{U}([0,2\pi))$, is used to re-sample the search curve:

$$y_n(s) = \frac{1}{2} + \frac{1}{\pi}\arcsin(\sin(\omega_n s + \psi_n)). \tag{13}$$

Further, ω_n is assigned one value (high) while the remaining variables $\Omega\setminus\omega_n$ are given another (low). In this manner by evaluating for $\Omega\setminus\omega_n$ the total sensitivity is obtained.

2.3.3. Generalised polynomial chaos using sparse grids

The use of global polynomial approximations is promising when the quantity of interest $u(\mathbf{y})$ is smooth with respect to the random input variables $\{y_n\}$.

The tensor product structure of $L_\rho^2(\Gamma)$ allows one to introduce a polynomial subspace of $L_\rho^2(\Gamma)$ denoted by $\mathbb{P}(\Gamma)$ as well as $\rho(\mathbf{y})\,\mathrm{d}\mathbf{y}$-orthonormal basis

$$\Psi_{\mathbf{p}}(\mathbf{y}) = \prod_{n=1}^{N} \Psi_{p_n}(y_n), \quad \mathbf{p} = (p_1, p_2, \ldots, p_n, \ldots, p_N) \in \mathbb{N}^N, \tag{14}$$

where $\Psi_{p_n}(y_n)$ denotes $\rho(y_n)\,\mathrm{d}y_n$-orthonormal polynomials on Γ_n. The goal is to project $u(\mathbf{y})$ on $\mathbb{P}_{\Lambda(\omega)}(\Gamma) = span\{\Psi_{\mathbf{p}}(\mathbf{y}),\ \mathbf{p} \in \Lambda(\omega)\}$ to obtain a global polynomial approximation

$$u_\omega(\mathbf{y}) = \sum_{\mathbf{p} \in \Lambda(w)} \alpha_{\mathbf{p}} \Psi_{\mathbf{p}}(\mathbf{y}), \tag{15}$$

for a suitable $\{\Psi_{\mathbf{p}}\}_{\mathbf{p} \subseteq \Lambda(\omega)}$, where $\Lambda(\omega), \omega \in \mathbb{N}$ are polynomial spaces of increasing index sets with respect to ω. This representation is known as a gPC expansion [19,51].

In a computational context the gPC expansion needs to be truncated, and here the general construction of $\Lambda(\omega)$ provides a polynomial space hierarchy with ω. The classical Tensor Product polynomial space $\Lambda(\omega) = span\{\mathbf{p} \in \mathbb{N}^N : \max_{n=1,2,\ldots,N} p_n \leq \omega\}$ suffers from the curse of dimensionality since its dimension increases exponentially fast with the number N of random input variables. A more attractive option is the *sparse* Total Degree polynomial space $\Lambda(\omega) = span\{\mathbf{p} \in \mathbb{N}^N : \sum_{n=1}^{N} p_n \leq \omega\}$. The choice and construction of $\Lambda(\omega)$ are discussed in detail in [2].

When the randomness in $\mathbf{y}$ is described by certain probability distributions, the Sobol' indices can be determined *exactly* from the coefficients of the gPC expansion of $u(\mathbf{y})$. This is true when described by for example the uniform and normal distribution. When computing statistical moments such as the expected value and variance of $u(\mathbf{y})$ the appropriate family of $\rho(\mathbf{y})\,\mathrm{d}\mathbf{y}$-orthonormal polynomials should be chosen with respect to the distribution measure of the input variables (see [50]). Many common probability distributions correspond to classical real orthogonal polynomials given in the general Askey scheme. Even in cases when the underlying probability distribution of y_n is not represented in the general Askey scheme, y_n can be parametrised by

a finite number of uniformly distributed variables through an appropriately chosen non-linear transformation following the theory of copulas (see [31]).

As the random variables in this study are uniformly distributed the normalised Legendre polynomials are used. The first and second statistical moments of $u_\omega(\mathbf{y})$ are then directly obtained from the gPC coefficients $\{\alpha_\mathbf{p}\}$:

$$\mathbb{E}[u_\omega(\mathbf{y})] = \alpha_\mathbf{0} \quad \text{and} \quad \mathbb{V}[u_\omega(\mathbf{y})] = \sum_{\mathbf{p} \in \Lambda(\omega)} \alpha_\mathbf{p}^2 - \alpha_\mathbf{0}^2. \tag{16}$$

There is a one-to-one correspondence between the analytical Sobol' indices and distinct subsets of gPC coefficients [44]: the gPC expansion of $u(\mathbf{y})$ may be recast as

$$\lim_{\omega \to \infty} u_\omega(\mathbf{y}) = \alpha_\mathbf{0} + \sum_{\mathbf{j} \subseteq \mathcal{J}} \sum_{\substack{\mathbf{p} \in \mathbb{N}^N: \\ i_n > 0 \Leftrightarrow n \in \mathbf{j}}} \alpha_\mathbf{p} \Psi_\mathbf{p}(\mathbf{y}), \tag{17}$$

and then given (1) and (17) the one-to-one correspondence is explicit, that is,

$$u_\mathbf{j}(\mathbf{y}_\mathbf{j}) = \sum_{\substack{\mathbf{p} \in \mathbb{N}^N: \\ p_n > 0 \Leftrightarrow n \in \mathbf{j}}} \alpha_\mathbf{p} \Psi_\mathbf{p}(\mathbf{y}_\mathbf{j}). \tag{18}$$

Insert Eq. (18) into the Sobol' index definition, (6), and exploit orthonormality of $\Psi_\mathbf{p}$ to conclude

$$S_\mathbf{j} = \frac{\sum_{\substack{\mathbf{p} \in \mathbb{N}^N: \\ p_n > 0 \Leftrightarrow n \in \mathbf{j}}} \alpha_\mathbf{p}^2}{\sum_{\mathbf{p} \in \mathbb{N}^N} \alpha_\mathbf{p}^2 - \alpha_\mathbf{0}^2}. \tag{19}$$

The gPC coefficients $\{\alpha_\mathbf{p}\}$ can in some cases be computed using Galerkin projection that involves a reformulation of the model equations [26], but this is impractical for deterministic models of complex structure, such as those involving non-linear governing equations. To circumvent this, the non-intrusive stochastic sparse grid collocation method [1] devised by Smolyak [39] can be applied. Other non-intrusive approaches are described elsewhere [26], for example those based on projection, that determine the coefficients by integration, and regression-based approaches, that rely on least squares.

Stochastic sparse grid collocation methods build upon a set of collocation points $\{\mathbf{y}_k \in \Gamma\}$ with corresponding function responses $\{u(\mathbf{y}_k)\}$, a global polynomial approximation $u_\omega : C^0(\Gamma) \to \mathbb{P}_{m(\mathbf{i})-1}(\Gamma)$:

$$u_{SG,\omega}(\mathbf{y}) = \sum_{\mathbf{i} \in \mathcal{I}(\omega)} c(\mathbf{i}) \bigotimes_{n=1}^{N} U_n^{m(i_n)}[u](\mathbf{y}),$$
$$c(\mathbf{i}) = \sum_{\substack{\mathbf{j} = \{0,1\}^N \\ \mathbf{i}+\mathbf{j} \in \mathcal{I}(\omega)}} (-1)^{|\mathbf{j}|}, \tag{20}$$

where $U_n^{m(i)} : C^0(\Gamma_n) \to \mathbb{P}_{m(i)-1}(\Gamma_n)$ denotes a mono-dimensional Lagrangian polynomial interpolant operator, $\otimes_{n=1}^N$ the Cartesian tensor product operator of the sets of collocation points in each direction n, $\mathbf{i} \in \mathbb{N}_+^N$ multi-indices, $\mathcal{I}(\omega)$ a sequence of increasing index sets and $m(i)$ the number of collocation points used to build the mono-dimensional interpolant at level i. The polynomial approximation (20) is known as sparse grid approximation and its construction is described elsewhere [4].

The set of indices $\mathcal{I}(\omega)$ can be chosen so that the approximation belongs to a given polynomial space $\Lambda(\omega)$ [2]. This study will use the isotropic Smolyak sparse grid which is defined by

$$\mathcal{I}_{\text{Smolyak}}(\omega) = \left\{ \mathbf{i} \in \mathbb{N}_+^N : \sum_{n=1}^{N} (i_n - 1) \le \omega \right\} \tag{21}$$

and

$$m(i) = \begin{cases} 2^{i-1} + 1, & i > 1, \\ 1, & i = 1. \end{cases} \tag{22}$$

When using the Smolyak sparse grid many of the coefficients $c(\mathbf{i})$ in (20) may be zero, hence the name *sparse grid*. In this study the mono-dimensional Lagrangian interpolants use the non-nested Gauss–Legendre rule so that the gPC expansion is built upon tensor products of Legendre polynomials. The collocation points used in a Smolyak sparse grid with the Gauss–Legendre rule are shown in Fig. 2. Keep in mind that generally the sparse grid approximation (20) is not interpolatory [3], unless it is constructed using a nested rule for the collocation points, e.g. Clenshaw–Curtis points.

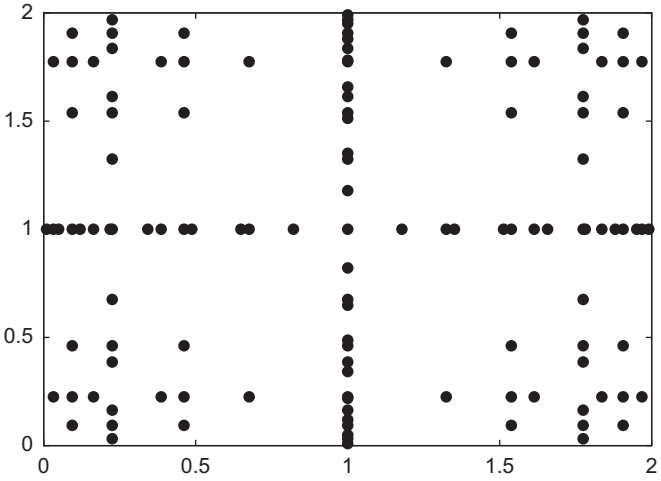

Fig. 2. 2-D example of a Smolyak sparse grid $\omega = 4$ using Gauss–Legendre points.

Using direct sparse grid quadrature requires the evaluation of high-dimensional integrals to obtain the gPC coefficients, to circumvent this the key is to convert the sparse grid approximation into a Legendre gPC expansion without the need to evaluate any high-dimensional integrals (see [45]).

2.4. Numerical tests

In this section we first evaluate the methodologies for global sensitivity introduced earlier (i.e. Monte Carlo, EFAST and gPC). The method performing most accurately with fewest number of function evaluations is then applied to the analysis of the variation of CO_2 outflow rate with composition.

The methodologies are applied to two test functions for which the analytical Sobol' indices are known exactly. Formulas to calculate the analytical Sobol' indices for these functions can be found in [13]. A further test function is constructed to investigate the performance of the methods under varying levels of difficulty, where the steep changes involved can be made nearly discontinuous.

2.4.1. Ishigami function

The Ishigami test function is given in Saltelli et al. [37]:

$$u(\mathbf{y}) = \sin(y_1) + 7\sin^2(y_2) + 0.1 y_3^4 \sin(y_1), \tag{23}$$

where $y_n \sim \mathcal{U}([-\pi, \pi])$, that is, uniformly distributed in $[-\pi, \pi]$. A fourth dummy input which is not used in the function evaluation is also used in the analysis.

Fig. 3a–d shows a comparison of the convergence performance for each of the methods for S_1, S_2, S_1^T and S_2^T. As may be observed in the cases of S_1, S_1^T and S_2^T, the behaviour obtained using the MC and QMC is not markedly different, while EFAST shows no sign of further convergence. In contrast, the gPC converges to machine precision within ca. 10,000 function evaluations. The gPC shows a similar rate of convergence for S_2 (Fig. 3b), while in this case EFAST shows a markedly better convergence, performing significantly better than both the MC and QMC.

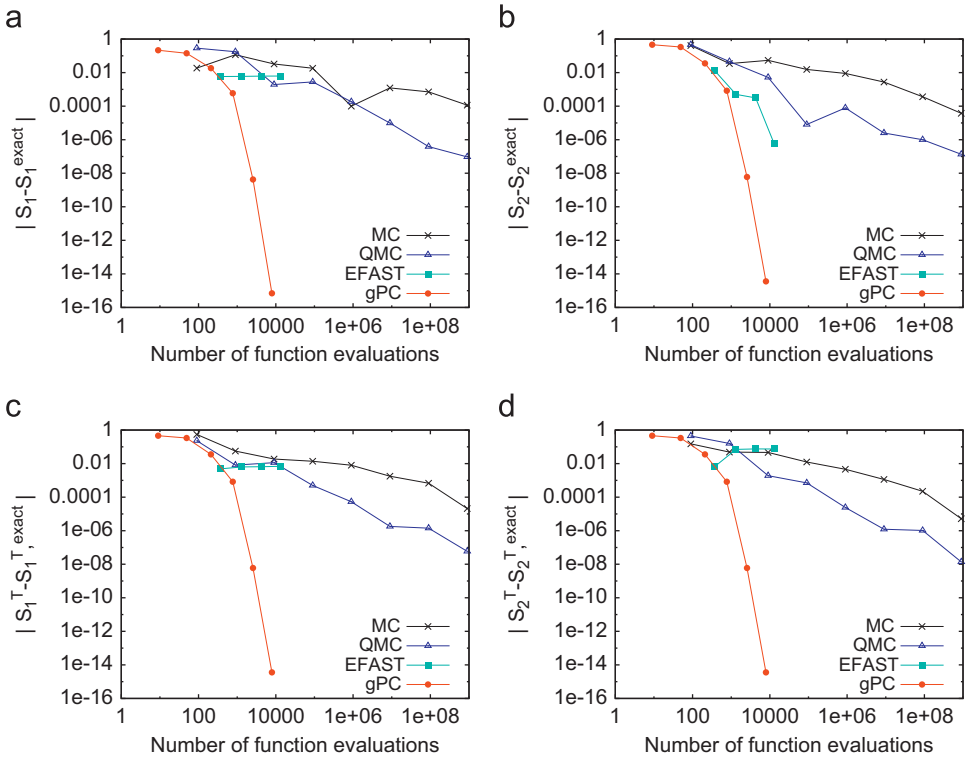

Fig. 3. Error convergence of sensitivity indices of the Ishigami function: (a) S_1, (b) S_2, (c) S_1^T, (d) S_2^T.

The excellent performance of the gPC for the Ishigami function is unsurprising given that while the function is non-linear, it is smooth and so an approximation by polynomials to arbitrary degree is possible.

2.4.2. Sobol' test function

In order to evaluate the performance for anisotropic non-smooth functions and higher dimensional input data, the following example is utilised [5]:

$$u(\mathbf{y}) = \prod_{n=1}^{8} \frac{|4y_n - 2| + a_n}{1 + a_n}, \tag{24}$$

where $a_1 = 0$, $a_2 = 2$, $a_3 = 5$, $a_4 = 10$, $a_5 = 20$, $a_6 = 50$, $a_7 = 100$ and $a_8 = 500$ and $y_n \sim \mathcal{U}([0,1])$, $n = 1, \ldots 8$.

Fig. 4a–d shows a comparison of the convergence performance for each of the methods for S_1, S_2, S_1^T and S_2^T. As may be observed in each case, the performance of the gPC is again better than for the other methods tested, though this is not as marked as in the case of the Ishigami function. Additionally, the values obtained for S_1, S_1^T, and S_2^T using EFAST appear not to converge to their analytical solutions. Thus the results indicate that even for a function for which the gPC is not ideally suited, it still achieves an accuracy equivalent or better than that obtained using the other standard methodologies.

2.4.3. Rapid Change test function

To further explore the level of rapid change up-to-which the gPC is still advantageous we construct a family of multi-variate test functions (that used by [43] extended to multi-dimensions) with two regions of rapid change:

$$u(\mathbf{y}) = 1 - \frac{1}{1 + \exp(-b_1(\sum_{n=1}^{N}(c_n y_n - w_1))} + \frac{4}{5(1 + \exp(-b_2(\sum_{n=1}^{N}(c_n y_n - w_2)))}, \tag{25}$$

where $y_n \sim \mathcal{U}([-1,1])$. Here $\mathbf{c} = (c_1, c_2, \ldots, c_N)$ are parameters satisfying $\Sigma_{n=1}^{N} c_n = 1$, whereas $\mathbf{w} \in [-1,1]^2$ can be interpreted as the positioning of two regions of rapid (exponential) changes. The difficulty of the function is in turn controlled by the magnitude of $\mathbf{b} \in (0, +\infty)^2$, see Fig. 5a. Fig. 5b shows the same case in the presence of additive white noise, intended to represent the numerical error which is present in complex simulations, i.e. $u(\mathbf{y}) + \varepsilon(\mathbf{y})$, $\varepsilon(\mathbf{y}) \sim \mathcal{N}(0, \sigma^2)$.

Fig. 6a–d shows the comparison of behaviour for values of $\mathbf{b}$ of (10,30), (10,75), (10,150) and (75,150), respectively. As may be observed in Fig. 6a, representing the least difficult function, the rate of convergence of the gPC is superior to that of both the MC and QMC, reaching reasonable accuracy in under 1000 function evaluations. As the magnitude of $\mathbf{b}$ increases (Fig. 6b–d) it is clear that the performance of the gPC becomes progressively worse. For the most difficult problem, that is where $\mathbf{b}$ is (75,150) (Fig. 6d), the results do not show any sign of convergence.

Fig. 7a–d again shows the convergence behaviour of the three methodologies using σ values of 0, i.e. without noise, 0.005, 0.01 and 0.05, respectively. As expected, as the degree of noise applied grows the performance of the gPC is observed to deteriorate, and for the larger σ values (Fig. 7c and d) the results fail to converge. Same behaviour has been observed for the other first order effects. The reduction in size of the first order Sobol' indices is because the non-linear gPC coefficients grow, and the linear gPC coefficients remain the same, as the noise level increases. In these cases it is clear that the gPC is not applicable.

It is important to note that the highest level of noise ($\sigma = 0.05$) is much larger than that expected to occur in a numerical model. In particular, for the application that is considered in this work we do not expect the extremely rapid changes or high level of noise

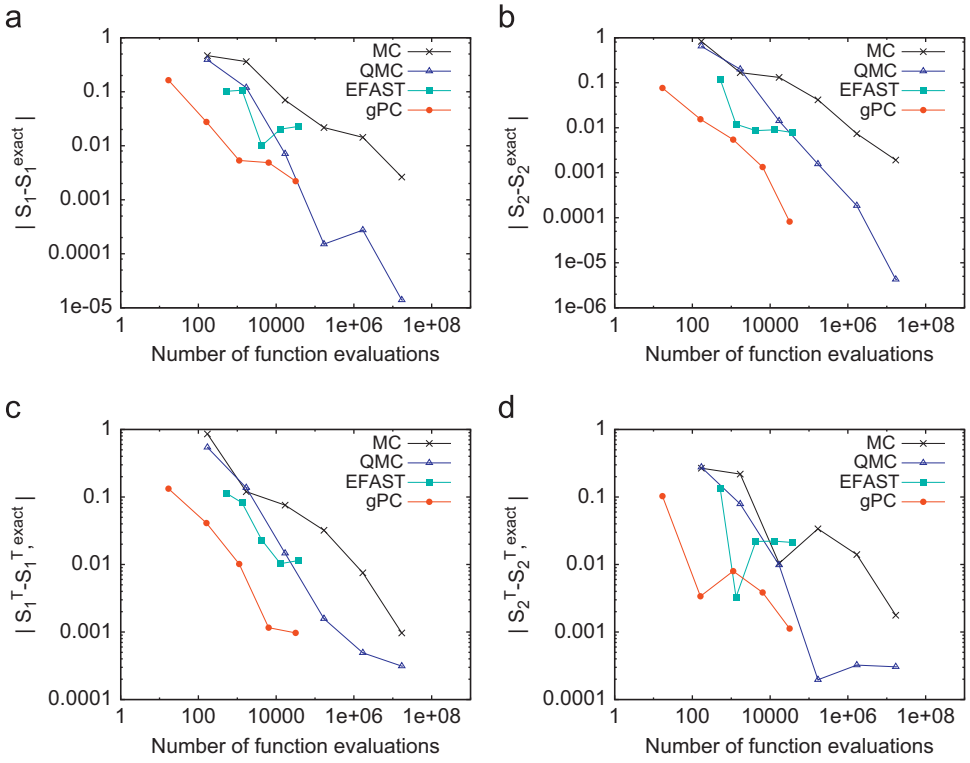

Fig. 4. Convergence of sensitivity indices of the Sobol' test function: (a) S_1, (b) S_2, (c) S_1^T, (d) S_2^T.

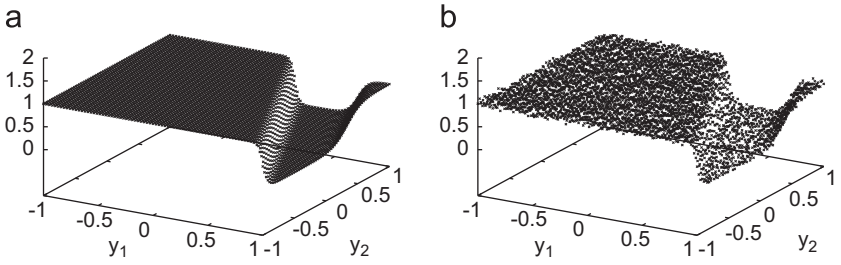

Fig. 5. Rapid Change function (25) with and w/o additive noise, where $\mathbf{c}=(0.3,0.7)$, $\mathbf{w}=(0.4,0.8)$, and $\mathbf{b}=(75,30)$: (a) Rapid Change function and (b) Rapid Change function with additive white noise $\sim\mathcal{N}(0,\sigma^2),\sigma=0.05$.

that caused the failure of the gPC. This was also verified by taking random walks in the input space as described in Section 3.2.2.

2.4.4. Discussion

From the above test cases it has been shown that even in cases where the underlying function contains steep gradients and low levels of noise the gPC technique outperforms the other methods tested. In particular, accurate results are obtainable with gPC within a very limited budget of function evaluations, whereas MC and QMC are, due to slow convergence, impractical for computationally expensive functions. Hence, unless there are known function characteristics that suggest its inadequacy, such as a high level of numerical noise, this technique should be attempted before resorting to the other methods presented.

3. Application: pressurised CO_2 pipeline failure

In the previous section it was found that gPC using sparse grids provided an efficient means to calculate the Sobol' indices for GSA. In what follows this technique is applied to the study of the impact of impurities stream on the outflow following the failure of a pressurised CO_2 pipeline.

In practice the composition will be dependent on the capture method (i.e. pre-combustion, post-combustion or oxyfuel) and the post-capture processing. As part of a complex CCS network, the mixing of CO_2 streams, each containing various levels of impurities, naturally introduces a great amount of uncertainty as to the overall composition of the fluid being transported. The composition of the CO_2 stream will, however, have to comply with the prevailing legislative limits [17].

Preliminary analyses of the impact of impurities on the CO_2 decompression behaviour resulting from pipeline failure have been made [7,11]. Likewise in the case of fracture, testing of the effect of impurities on crack propagation has been limited to representative mixtures for each of the capture methods [29]. Both cases suggest that the composition of the CO_2 mixture has a dramatic impact on the consequences of pipeline failure.

Hence, a quantification of the sensitivity of the consequences of pipeline failure to the CO_2 stream composition is a matter of great current concern. Importantly, due to the complex thermodynamic behaviour of multi-component CO_2 mixtures, it is unlikely that the effects will be linear and so not amenable to

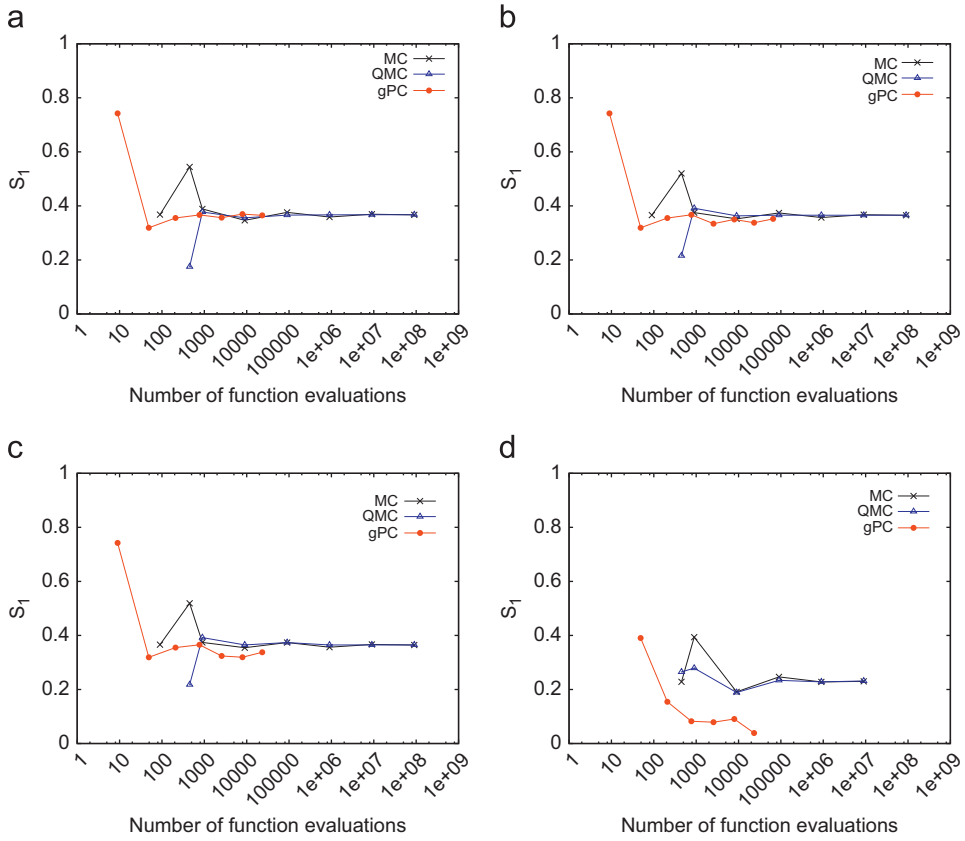

Fig. 6. Calculated sensitivity indices of the Rapid Change function for different **b**, where $\mathbf{w}=(0.4,0.8)$ and $\mathbf{c}=(0.4,0.3,0.2,0.1)$: (a) S_1, with $\mathbf{b}=(10,30)$; (b) S_1, with $\mathbf{b}=(10,75)$; (c) S_1, with $\mathbf{b}=(10,150)$; (d) S_1, with $\mathbf{b}=(75,150)$.

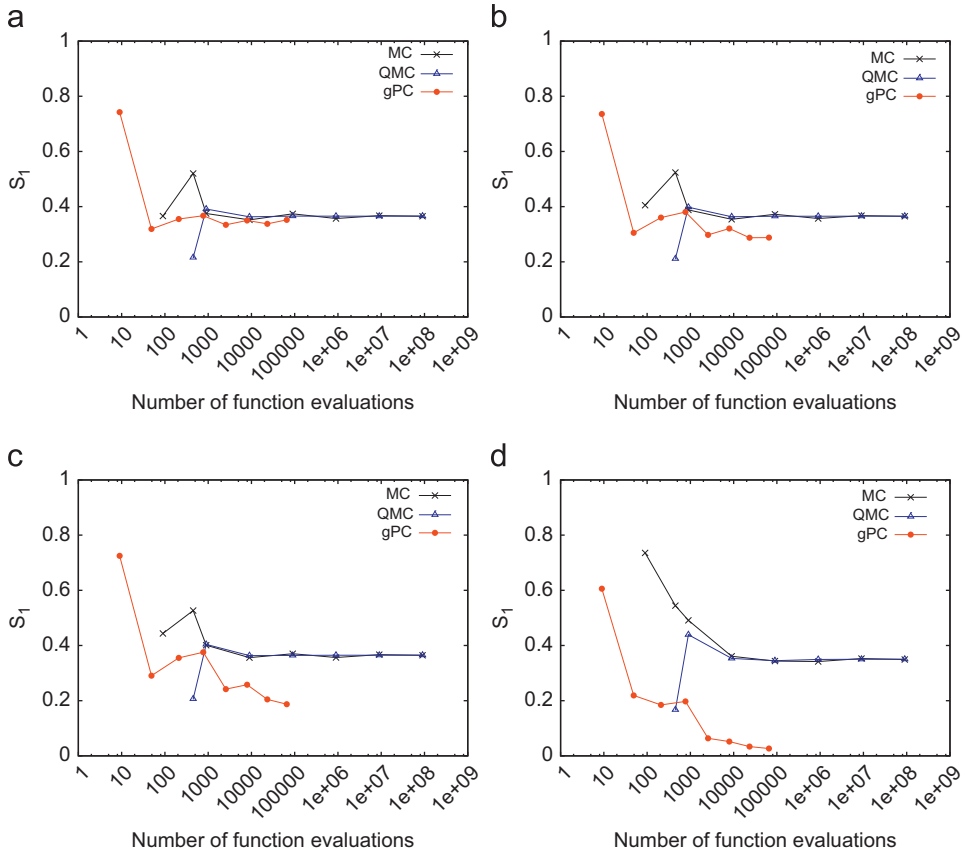

Fig. 7. Convergence of sensitivity index S_1 of the Rapid Change function for different levels of additive noise $\varepsilon(\mathbf{y})\sim\mathcal{N}(0,\sigma^2)$, where $\mathbf{b}=(10,75)$, $\mathbf{w}=(0.4,0.8)$ and $\mathbf{c}=(0.4,0.3,0.2,0.1)$: (a) w/o additive noise, (b) $\sigma=0.005$, (c) $\sigma=0.01$, (d) $\sigma=0.05$.

OAT analysis. As such, the application of efficient methods GSA offer important insights.

3.1. Pipeline decompression model

The full background theory of the fluid flow model employed in this study to predict the decompression behaviour, implemented in the CFD code PipeTech including its validation against real pipeline rupture data is given elsewhere [27,28,32]. For completeness, a brief account of its main features is given here. Based on the homogeneous flow assumption, in the case of unsteady, mono-dimensional flow the mass, momentum and energy conservation equations, respectively, are given by

$$\frac{D\rho}{Dt}+\rho\frac{\partial u}{\partial x}=0, \tag{26}$$

$$\rho\frac{Du}{Dt}+\rho u\frac{\partial u}{\partial x}+\frac{\partial P}{\partial x}-\alpha=0, \tag{27}$$

$$\rho\frac{Dh}{Dt}-\frac{DP}{Dt}-(q-u\beta)=0, \tag{28}$$

where D/Dt is the material derivative and r, u, P and h are the density, velocity, pressure and specific enthalpy of the homogeneous fluid as a function of time, t, and space, x. q is the heat transferred through the pipe wall to the fluid and β is the friction force term

$$\beta=-2\frac{f_w}{d}\rho u|u|, \tag{29}$$

where f_w is the Fanning friction factor and d the pipeline diameter. Also,

$$\alpha=\beta-\rho g\sin\theta, \tag{30}$$

where θ is the angle of inclination of the pipeline to the horizontal.

Eqs. (26)–(28) are quasi-linear and must be solved numerically. As described elsewhere, the method of characteristics (MOC) [52] is used as the numerical solution method. At the boundary representing the release plane the choked flow condition [15] is applied using the methodology described in Wong and Mahgerefteh [48]. The Peng Robinson equation of state [34] is employed to generate the relevant vapour/liquid equilibrium data required for the outflow model.

3.2. Impact of impurities on CO_2 pipeline decompression

A number of studies have sought to define maximum allowable concentrations of impurities in CO_2 streams for pipeline transportation [14,17,33]. Table 1 summarises the compositions suggested by Dynamis [14] and Ecofys [20].

Table 1
CO_2 quality recommendations from the Dynamis project and the Ecofys study.

Species	Dynamis	Ecofys
CO_2	$>95.5\%$	$>95\%$
N_2, O_2, H_2, Ar, CH_4	4 vol% max (no individual $>2\%$)	4 vol% max (cumulative)
H_2O	500 ppm	<500 ppm
SO_x	100 ppm	–
NO_x	100 ppm	–
H_2S	200 ppm	–
CO	2000 ppm	No data

For the sake of this analysis a simplified composition is assumed in which the only non-CO_2 components present are N_2, CH_4 and O_2. Further it is assumed, in accordance with Table 1, each component's mole percentage is a uniformly distributed random variable, $y_n\sim\mathcal{U}([0,2])$. Furthermore, zero correlation between the random variables is assumed. It is envisaged that as planning for CCS networks progresses a better definition of the uncertainty in the composition will be available for analysis.

As described previously, the release behaviour and its variation with time following pipeline failure dictates the resulting atmospheric dispersion of the escaping inventory. A large number of variables are required to define the fluid release including the thermodynamic properties (e.g. pressure, temperature), phase distribution and outflow rate. In order to simplify the study, the effect of the forward propagation of uncertainty in the composition is assessed by the probability distribution of the outflow rate, as is commonly the case in the literature [23]. The following represents the results of the application of the methodology described above to an hypothetical example involving the full bore rupture at the end of a highly pressurised pipeline carrying a CO_2 mixture with small amounts of impurities. Table 2 shows the pipeline characteristics and prevailing conditions. In order to reduce the computational expense of each outflow simulation the length of the pipeline is restricted to 1 km. An equidistant grid system comprising 100 nodal points is employed for the spatial discretisation.

Table 2
Pipeline characteristics and prevailing conditions.

Pipeline characteristics	
Pipeline length (km)	1
External diameter (mm)	609.4
Wall thickness (mm)	9.45
Pipe wall roughness (mm)	0.05
Initial conditions	
Feed temperature (K)	288.15
Ambient temperature (K)	288.15
Feed pressure (bara)	150
Ambient pressure (bara)	1.01

For GSA we are investigating the impact of impurities for the first 80 s following a pipeline failure. In contrast for UQ, to afford a larger number of simulation runs using MC, the simulated time is reduced to 1 s, and hence serves as an analysis of the impact of impurities at this early stage of depressurisation.

3.2.1. Uncertainty analysis

An MC computation using a sample size of 10,000 was performed taking samples from the independent joint distributions of y_n representing the space of possible compositions. Fig. 8 shows the binning of the resulting samples that approximates the shape of the probability distribution at 1 s after the pipeline failure. As may be observed, the distributions range of ca. 1200 kg/s shows that relatively small variations in the composition have an important impact on the outflow rate. Such differences have been observed to have significant implications for the dispersion behaviour of the resulting cloud [47].

Table 3 contains a summary of the statistical data, including the calculated mean and standard deviation. As may be observed from the table, the wide dispersion of the data in Fig. 8 is borne out by the standard deviation of 186.2 kg/s.

Fig. 9a–c show scatter plots of the variation of discharge rate at 1 s following pipeline failure with percentage mole fraction of CH_4, N_2 and O_2, respectively. It is immediately clear from Fig. 9a that there is a negligible correlation between concentration

of CH_4 and the outflow rate. In contrast, the same plot for N_2 (Fig. 9b) indicates an almost linear relationship with the equivalent data for O_2 (Fig. 9c) showing a similar, albeit weaker, behaviour.

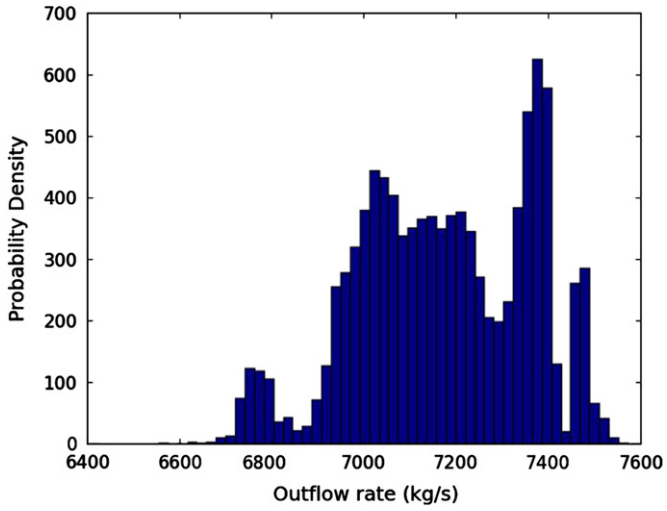

Fig. 8. Probability distribution of outflow rate.

Table 3
Data summary.

Quantity	
Mean	7174.6
Standard deviation	186.2
Median	7175.3
Highest percentile	7493.4

3.2.2. Sensitivity analysis

Given the good performance of the gPC in the calculation of the Sobol' indices described in Section 2.3 this method was applied to the CO_2 outflow rate problem outlined previously. Table 4 shows the first and total effects obtained from this analysis. As may be observed the calculated first order effects for variable N_2 do not appear to show convergent behaviour with the increasing number of samples used. Similar behaviour is also seen for the other variables.

In order to understand the behaviour of the system a linear path with randomly selected end points in the input space was generated and sampled along. Fig. 10a shows the outflow rate at 1, 5 and 30 s along the path, while Fig. 10b shows the same results for 1 and 5 s at a different scale. As may be observed in Fig. 10a, the results appear to be relatively smooth for each of the presented times. In contrast in Fig. 10b it is clear that, particularly at 1 s, there are small oscillations, which are expected due to the extreme dependence on the composition at this early stage of the depressurisation. Importantly, these errors do not affect the qualitative behaviour of the model.

Table 4
First order and total effects of the CO_2 outflow rate after 30 s using gPC.

Evaluations	First order effects			Total effects		
	N_2	CH_4	O_2	N_2	CH_4	O_2
7	0.583104	0.146179	0.270718	0.583104	0.146179	0.270718
31	0.590446	0.158301	0.249544	0.591767	0.158918	0.251024
111	0.623149	0.146523	0.220663	0.629544	0.152329	0.228095
351	0.556694	0.182115	0.247479	0.566068	0.191203	0.258142
1023	0.608691	0.133408	0.232031	0.627223	0.152822	0.250330
2807	0.557299	0.156367	0.259222	0.578916	0.178203	0.280186

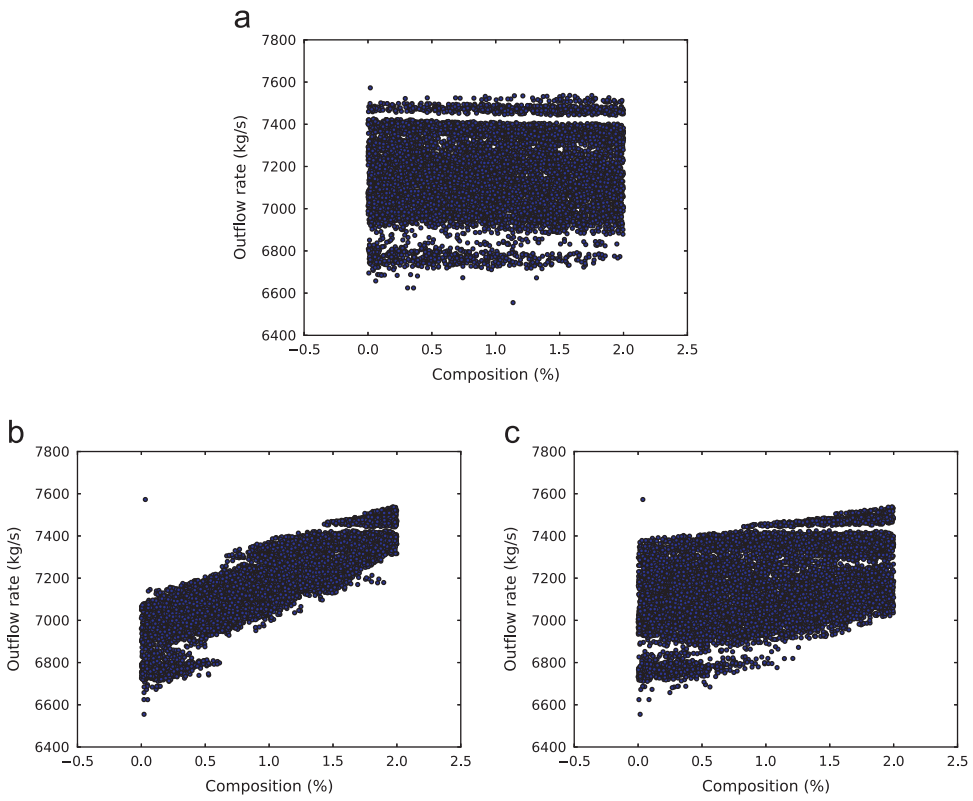

Fig. 9. Variation of flowrate with impurity fraction: (a) CH_4, (b) N_2, (c) O_2.

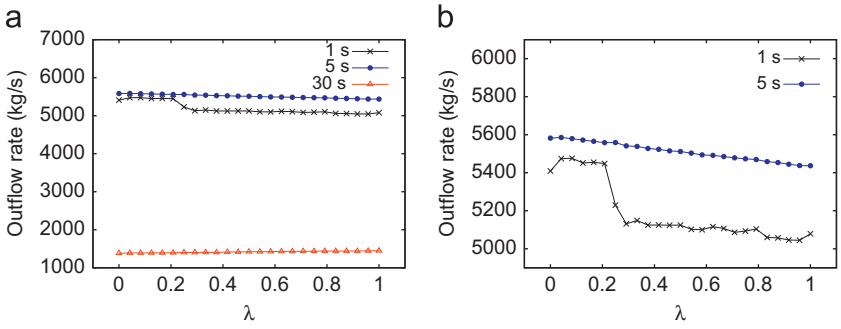

Fig. 10. Visualisation of outflow rate response along the linear path $\mathbf{y} = \mathbf{y}_1 + \lambda(\mathbf{y}_2 - \mathbf{y}_1)$, $\lambda \in [0,1]$ between two distant points $\mathbf{y}_1$ and $\mathbf{y}_2$ in the input domain of the random variables, Γ: (a) path walk at 1 s, 5 s, and 30 s; (b) path walk magnified for 1 s and 5 s to visualise non-smooth behaviour at 1 s.

Table 5
Magnitude of the linear gPC coefficient against the total sum of gPC coefficients, for each variable, after 30 s.

Evaluations	Linear gPC			Total gPC		
	N_2	CH_4	O_2	N_2	CH_4	O_2
7	112.1	56.31	76.62	124.5	58.13	79.74
31	116.0	59.92	75.42	126.2	68.74	77.51
111	117.1	56.78	69.56	151.0	73.06	75.18
351	113.0	64.58	75.18	157.8	96.92	109.1
1023	116.9	54.44	72.26	193.8	129.0	130.4
2807	112.23	59.10	76.38	240.5	163.7	194.2

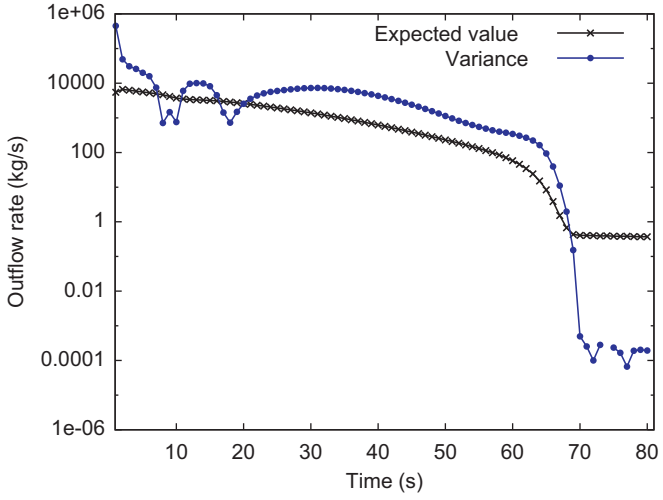

Fig. 11. Variation of $\mathbb{E}[u(\mathbf{y})]$ and $\mathbb{V}[u(\mathbf{y})]$ with time.

Notwithstanding the above, it is clear from Table 4 that both the ranking of the impact of the variables and the magnitude of the effects remain the same for all the sample sizes tested. Given this behaviour, the approximation of the Sobol' indices obtained with just 7 points appears to give a reasonable estimate of the indices and their ordering. For the purposes of comparison, MC and QMC simulations of similar sizes to those described in Table 4 were also performed, however, these failed to produce meaningful results.

Further, for the results obtained (for all sample sizes), N_2 has the largest first effect followed by O_2 and CH_4. The results presented in Table 5 agree with the linear behaviour found by the relevant scatter plot (Fig. 9b), and also show that the non-linear behaviour captured by the gPC coefficients grows as the level of the sparse grid approximation used by the gPC increases.

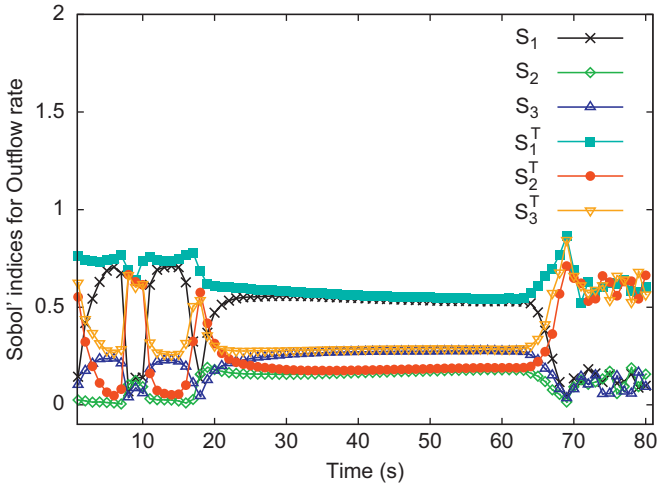

Fig. 12. Variation of Sobol' indices with time, using a sample size of 2807.

Additionally, as the first effect is almost equal to the total effect for all components, the impact of the interaction between the impurities is extremely limited.

Given the highly transient nature of pipeline decompression it is expected that the impact and importance of the impurities will be a function of time. Fig. 11 shows the variation of $\mathbb{E}[u(\mathbf{y})]$ and $\mathbb{V}[u(\mathbf{y})]$ with respect to time. As may be observed, $\mathbb{E}[u(\mathbf{y})]$ shows a slow decline for approximately 64 s, when the drop becomes more rapid before reaching a constant value of almost 0 kg/s indicating that the release has reached ambient pressure. The $\mathbb{V}[u(\mathbf{y})]$ shows similar behaviour except between ca. 10 and 20 s where there appear to be oscillations in the variance. This region of the physical problem is characterised by rapid phase changes, and so it is anticipated that these fluctuations are due to the differing phase equilibria of the CO_2 mixtures. For the period after ca. 64 s, as the flow rate is negligible the changes in composition produce a very small variance.

Fig. 12 shows the variation of the Sobol' indices with time calculated using a sparse grid of 2807 points. In Fig. 12, three distinct regimes of behaviour can clearly be observed:

1. The initial 20 s after rupture. During this stage the flow is dominated by rapid decompression inducing phase transitions that are complicated by the variation in the composition. This behaviour is expressed by the Sobol' indices through the fluctuations in their ordering and magnitude.
2. 20–64 s. In this range the outflow rate shows a steady decline, as a consequence the Sobol' indices approach both a constant

magnitude and ordering. Here the interaction between the components has little effect.
3. After 64 s. Here the pipeline rapidly decompresses resulting in the outflow dropping effectively to 0 kg/s and the composition has virtually no effect. Due to the very small variance in the system, the Sobol' indices calculated become less meaningful.

4. Conclusions

In the CCS chain, pressurised pipelines employed for the transportation of the captured CO_2 for subsequent sequestration will inevitably contain a range of stream impurities. The above presents a significant challenge given the established marked impact of the type and composition of the stream impurities on the safe and economical pipeline transportation of CO_2.

Predictive models utilised for design and risk assessment of such a system have been exploited for studying the sensitivity to such inherent variations. However, in the context of CO_2 pipeline transportation, given the very large number of potential variables, and the complexity of the models required, mean that the computational cost for a full global sensitivity analysis will be prohibitive.

In this paper commonly applied methods of GSA, i.e. MC, QMC and EFAST were first reviewed. Additionally, a gPC technique based on sparse grids was described. This formulation allows the simple evaluation of the Sobol' indices, while the sparse grid sampling greatly reduces the number of sample evaluations required.

These methodologies were then applied to two benchmark test problems found in the literature and a further problem constructed to replicate discontinuous behaviour. In the former the results indicated that the sparse grid based gPC method was able to achieve machine precision accuracy. For the latter problem it was observed that as the function became "rougher" the convergence rate decreased, and in the extreme case presented convergence was not observed. The addition of increasing levels of noise to this problem, used to replicate numerical error in computational simulations, showed that the gPC performed moderately well with low levels of noise, but again fails to converge as this was increased. In comparison the other methods tested require substantially larger sample sizes to achieve equivalent accuracy. On the other hand, as expected, the performance of MC/QMC was almost unaffected by the applied numerical noise. In summary, the gPC outperformed the other methods tested in all cases in terms of convergence per number of function evaluations, except in a single case where a very high level of noise was present.

The gPC technique was then applied to an analysis of an hypothetical pipeline failure under uncertainty in CO_2 mixture composition. An initial uncertainty analysis showed a variation in the outflow rate (after 1 s) of $>10\%$. Clearly, given that the outflow rate largely dictates the resulting dispersion, this level of variation has significant implications for the emergency response planning. Furthermore, scatter plotting showed that of the three impurities considered (N_2, CH_4 and O_2) only N_2 had a linear impact on the outflow rate.

The results of the gPC for the full decompression showed three distinct regimes of behaviour in which it was found that generally N_2 had the greatest impact on the outflow rate. In particular the second regime, in which the Sobol' indices show a relatively stable behaviour, appears to be the most for assessing the overall importance of each component.

In conclusion, it should be noted that the CO_2 impurities sensitivity analysis performed in this study primarily focused on pipeline transportation issues. Although in a wider context, the proposed sensitivity analysis could serve as part of a techno-economic analysis of the impact of impurities for the entire CCS chain.

Acknowledgements

The first and third authors would like to acknowledge the funding received from the European Union Seventh Framework Programme FP7-ENERGY-2009-1 under Grant agreement 241346. The second and fourth authors acknowledge the support of the Engineering and Physical Sciences Research Council (EPSRC) under Grant EP/G062129/1.

References

[1] Babuška I, Nobile F, Tempone R. A stochastic collocation method for elliptic partial differential equations with random input data. SIAM Review 2010;52(2):317–55.
[2] Bäck J, Nobile F, Tamellini L, Tempone R. Stochastic spectral Galerkin and collocation methods for PDEs with random coefficients: a numerical comparison. In: Hesthaven J, Rønquist E, editors. Spectral and high order methods for partial differential equations, Lecture notes in computational science and engineering, vol. 76. Springer-Verlag; 2011. p. 43–62 (selected papers from the ICOSAHOM '09 conference, Trondheim, Norway, 22–26 June 2009).
[3] Barthelmann V, Novak E, Ritter K. High dimensional polynomial interpolation on sparse grids. Advances in Computational Mathematics 2000;12(4):273–88.
[4] Beck J, Nobile F, Tamellini L, Tempone R. On the optimal polynomial approximation of stochastic PDEs by Galerkin and collocation methods. Mathematical Models and Methods in Applied Sciences 2012;22(09).
[5] Blatman G, Sudret B. Efficient computation of global sensitivity indices using sparse polynomial chaos expansions. Reliability Engineering and System Safety 2010;95:1216–29.
[6] Brown S. CFD Modelling of outflow and ductile fracture propagation in pressurised pipelines. PhD thesis, University College London; 2011.
[7] Brown S, Mahgerefteh H. From cradle to burial: high pressure phase equilibrium behaviour of CO_2 during CCS. In: Proceedings of the 2009 AIChE annual meeting; 2009.
[8] Bungartz H-J, Griebel M. Sparse grids. In: Acta numerica, vol. 13. Cambridge University Press; 2004. p. 849–54.
[9] Buzzard GT. Global sensitivity analysis using sparse grid interpolation and polynomial chaos. Reliability Engineering and System Safety 2012;107:82–9.
[10] Cea L, Bermúdez M, Puertas J. Uncertainty and sensitivity analysis of a depth-averaged water quality model for evaluation of *Escherichia Coli* concentration in shallow estuaries. Environmental Modelling & Software 2011;26(12):1526–39.
[11] Cosham A, Eiber RJ. Fracture control in carbon dioxide pipelines: the effect of impurities. In: 7th International pipeline conference (IPC2008), Calgary, 2008. p. 229–40.
[12] CPR. Guidelines for quantitative risk assessment—the 'Purple Book'. Committee for the Prevention of Disasters (CPR), The Hague, 1999.
[13] Crestaux T, Maître OL, Martinez J-M. Polynomial chaos expansion for sensitivity analysis. Reliability Engineering System Safety 2009;94(7):1161–72.
[14] Devisser E, Hendriks C, Barrio M, Molnvik M, Dekoeijer G, Liljemark S, et al. Dynamis CO_2 quality recommendations. International Journal of Greenhouse Gas Control 2008;2(4):478–84.
[15] Elias E, Lellouche G. Two-phase critical flow. International Journal of Multiphase Flow 1994;20(94):91–168.
[16] Ernst O, Mugler A, Starkloff H, Ullmann E. On the convergence of generalized polynomial chaos expansions. ESAIM: Mathematical Modelling and Numerical Analysis 2012;46(02):317–39.
[17] EU Communities. Implementation of directive 2009/31/ec on the geological storage of carbon dioxide. Technical report, EU Commission; 2011.
[18] Formaggia L, Guadagnini A, Imperiali I, Lever V, Porta G, Scotti A, Tamellini L. Global sensitivity analysis through polynomial chaos expansion of a basin-scale geochemical compaction model sparse tensor discretization of elliptic SPDEs. MOX-Report 2012-13, MOX, Dipartimento di Matematica, Politecnico di Milano, Milano; 2012.
[19] Ghanem RG, Spanos PD. Stochastic finite elements: a spectral approach. New York, USA: Springer-Verlag; 1991.
[20] Hendriks C, Hagedoon S, Warmenhoven H. Transportation of carbon dioxide and organisational issues of ccs in the Netherlands. Technical report, Ecofys; 2007.
[21] Homma T, Saltelli A. Importance measures in global sensitivity analysis of nonlinear models. Reliability Engineering and System Safety 1996;52(1):1–17.
[22] IPCC. IPCC special report on carbon dioxide and storage. Technical report, Intergovernmental Panel on Climate Change; 2005.
[23] Koornneef J, Spruijt M, Molag M, Ramírez A, Turkenburg W, Faaij A. Quantitative risk assessment of CO_2 transport by pipelines—a review of uncertainties and their impacts. Journal of Hazardous Materials 2010;177(May (1–3)):12–27.

[24] Kovscek AR, Wang Y. Geologic storage of carbon dioxide and enhanced oil recover. I. Uncertainty quantification employing a streamline based proxy for reservoir flow simulation. Energy Conversion and Management 2005;46: 1920–40.
[25] Kruse H, Tekiela M. Calculating the consequences of a CO_2-pipeline rupture. Energy Conversion and Management 1996;37(95):1013–8.
[26] Le Maître OP, Knio OM. Spectral methods for uncertainty quantification: with applications to computational fluid dynamics, Scientific computation. New York: Springer; 2010.
[27] Mahgerefteh H, Atti O. Modeling low-temperature-induced failure of pressurized pipelines. AIChE Journal 2006;52(3):1248–56.
[28] Mahgerefteh H, Atti O, Denton G. An interpolation technique for rapid CFD simulation of turbulent two-phase flows. Process Safety and Environmental Protection 2007;85(1):45–50.
[29] Mahgerefteh H, Brown S, Denton G. Modelling the impact of stream impurities on ductile fractures in CO_2 pipelines. Chemical Engineering Science 2012;74(May):200–10.
[30] McRae G, Tilden J. Global sensitivity analysis—a computational implementation of the fourier amplitude sensitivity test (fast). Computers Chemical Engineering 1982;6:15–25.
[31] Nelsen RB. An introduction to copulas (Lecture notes in statistics). 2nd ed. New York: Springer; 2006.
[32] Oke A, Mahgerefteh H, Economou I, Rykov Y. A transient outflow model for pipeline puncture. Chemical Engineering Science 2003;58:4591–694.
[33] Oosterkamp A, Ramsen J. State-of-the art overview of Co_2 pipeline transport with relevance to offshore pipelines. Technical report, PolyTec; 2008.
[34] Peng D-Y, Robinson DB. A new two-constant equation of state. Industrial & Engineering Chemistry Fundamentals 1976;15(1):59–64.
[35] Saltelli A, Annoni P. How to avoid a perfunctory sensitivity analysis. Environmental Modelling & Software 2010;25(12):1508–17.
[36] Saltelli A, Bolado R. An alternative way to compute Fourier amplitude sensitivity test (FAST). Computational Statistics & Data Analysis 1998;26(4): 445–460.
[37] Saltelli A, Chan K, Scott E. Sensitivity analysis. Chichester: John Wiley & Sons; 2000.
[38] Saltelli A, Tarantola S, Chan KP-S. A quantitative model-independent method for global sensitivity analysis of model output. Technometrics 1999;41(February (1)):39–56.
[39] Smolyak SA. Quadrature and interpolation formulas for tensor products of certain classes of unctions. Doklady Akademii Nauk SSSR 1963;4:240–3.
[40] Sobol' I. Quasi-Monte Carlo methods. Progress in Nuclear Energy 1990;24(1–3): 55–61.
[41] Sobol' I. Sensitivity estimates for nonlinear mathematical models. Mathematical Modeling & Computational Experiment 1993;1(4):407–14.
[42] Sobol' I. Global sensitivity indices for nonlinear mathematical models and their Monte Carlo estimates. Mathematics and Computers in Simulation 2001;55(1–3):271–80.
[43] Storlie C, Bondell H, Reich B. A locally adaptive penalty for estimation of functions with varying roughness. Journal of Computational and Graphical Statistics 2010;19(3):569–89.
[44] Sudret B. Global sensitivity analysis using polynomial chaos expansions. Reliability Engineering and System Safety 2008;93(July (7)):964–79.
[45] Tamellini L. Polynomial approximation of PDEs with stochastic coefficients. Ph.D. thesis, Politecnico di Milano; 2012.
[46] Weyl H. Mean motion. American Journal of Mathematics 1938;60:889–96.
[47] Witlox HWM, Stene J, Harper M, Nilsen SH. Modelling of discharge and atmospheric dispersion for carbon dioxide releases including sensitivity analysis for wide range of scenarios. Energy Procedia 2011;4:2253–60.
[48] Wong S, Mahgerefteh H. A numerical blowdown simulation incorporating cubic equations of state. Computers & Chemical Engineering 1999;23(9): 1309–1317.
[49] Xiu D, Hesthaven JS. High-order collocation methods for differential equations with random inputs. SIAM Journal on Scientific Computing 2005;27(3): 1118–1139.
[50] Xiu D, Karniadakis G. The Wiener–Askey polynomial chaos for stochastic differential equations. SIAM Journal on Scientific Computing 2002;24(2): 619–644.
[51] Xiu D, Lucor D, Su CH, Karniadakis GE. Stochastic modeling of flow–structure interactions using generalized polynomial chaos. Journal of Fluids Engineering 2002;124(1):51–9.
[52] Zucrow MJ, Hoffman JD. Gas dynamics. New York: Wiley; 1975.